PAPER

Studies of the dynamics of biological macromolecules using Au nanoparticle–DNA artificial molecules

Qian Chen,[abc] Jessica M. Smith,[ab] Haider I. Rasool,[bd] Alex Zettl[bd] and A. Paul Alivisatos*[ab]

The recent development of graphene liquid cells, a nanoscale version of liquid bubble wrap, is a breakthrough for *in situ* liquid phase electron microscopy (EM). Using ultrathin graphene sheets as the liquid sample container, graphene liquid cells have allowed the unprecedented atomic resolution observation of solution phase growth and dynamics of nanocrystals. Here we explore the potential of this technique to probe nanoscale structure and dynamics of biomolecules *in situ*, using artificial Au nanoparticle–DNA artificial molecules as model systems. The interactions of electrons with both the artificial molecules and the liquid environment have been demonstrated and discussed, revealing both the opportunities and challenges of using graphene liquid cell EM as a new method of bio-imaging.

Introduction

It has been a challenging goal in microscopy to visualize, and potentially modulate, the transformative kinetics of biomolecules during biological reactions at the nanometer resolution in their native liquid environment.[1-13] Such dynamics involving morphological details are critical to the functions of individual biological molecules, the feedback network of biological processes, and biomedical applications. For example, the folding and unfolding of proteins have inspired extensive theoretical and simulation efforts[2] to understand the molecular mechanisms of the exposing and hiding of active sites or binding pockets. In contrast, experimental efforts that can probe the conformational dynamics of biomolecules are largely limited, due to the lack of an imaging tool that can resolve *in situ* dynamics at the nanoscale.

[a]Department of Chemistry, University of California, Berkeley, CA 94720, USA. E-mail: alivis@berkeley.edu
[b]Materials Sciences Division, Lawrence Berkeley National Laboratory, Berkeley, CA 94720, USA
[c]Miller Institute for Basic Research in Science, University of California, Berkeley, CA 94720, USA
[d]Department of Physics, University of California, Berkeley, CA 94720, USA

The previous focus in the development of experimental approaches has been on two strategies, both of which have had great successes, as well as limitations: pushing the spatial resolution for dynamic imaging techniques, such as super-resolution optical microscopy,[5,14,15] and pushing the dynamic capability for high spatial resolution techniques, such as cryo EM[1] and X-ray crystallography.[3,4] Super-resolution optical microscopy, in its various forms, can have a record spatial resolution of ~15 nm, achieved usually by fitting the point spread function of the emission of individual fluorescent labels. This mechanism of imaging already has its own limitation: the morphology of a biomolecule can only be generated when the whole biomolecule is covered with labeling agents, which is not experimentally easy and also poses complications in possible interference effects from labeling agents. On the other hand, cryo EM has developed a suite of imaging and analysis techniques that can generate the three-dimensional (3D) shape of biomolecules at sub nm resolution. However, TEM (transmission electro microscopy) was considered to be incompatible with the existence of a liquid sample, and thus dynamics in liquid, due to its high vacuum working condition. In cryo EM techniques, therefore, the biological samples are embedded in vitri-fied ice, leaving only snapshots of the conformational states of biomolecules along their dynamic trajectory during reactions. X-ray crystallography shares similar limitations, with the additional constraint that it can work only on the crystalline forms of biomolecules. This constraint is more pronounced when the relevant functional states of the biomolecules are not necessarily their bulk crystalline forms. For example, membrane proteins are still presented as a great challenge for X-ray crystallography, since they function and transform in close proximity with the cellular membrane.

Here we investigate the opportunities and challenges of a third strategy towards the elusive nanoscale dynamics in biological systems: graphene liquid cell TEM, with the unique advantage of retaining a native liquid environment and the capability of capturing continuous dynamics at nanometer resolution.[13,16] In principle, graphene liquid cell TEM integrates the powers of the previous two approaches and can thus probe a large sample space that has not been approachable before in bio-imaging. It allows samples to remain in a liquid environment, like super-resolution optical microscopy, but can also reveal biomolecular morphological details. It has ultrahigh spatial resolution, just like cryo EM and X-ray crystallography, but now the samples are in their native liquid environment. In comparison to the conventional thick-walled liquid phase EM strategies using Si_3N_4 to hold liquid against high vacuum,[17–21] graphene liquid cells wrap a liquid samples using two graphene layers and seal the sample *via* the van der Waals force between two graphene layers. In this liquid cell configuration, we can minimize the loss of imaging electrons from the one-atom thick graphene window. The atomic resolution imaging capability of EM can thus be maintained, despite the liquid molecules surrounding the sample, which is potentially crucial for the observation of low atomic number biological samples in liquid. The van der Waals sealing between the graphene layers can also minimize possible contamination resulting from adhesive spacers.

Meanwhile, the traditionally identified complication with high spatial reso-lution imaging techniques can persist here: the probing beams, electron beam or X-ray, have high energy that interacts with, and sometimes damages, the sample being imaged. This complication is an important concern in the broad use of

liquid phase EM in imaging nanoscale dynamics of biomolecules. However, graphene has its own unique properties that make it more advantageous than other window materials for liquid phase EM. Our earlier work,[13] as well as other recent independent research,[9,22,23] has observed that graphene can help increase the electron beam tolerance of samples, such as an inorganic MoS_2 lattice and ferritin molecules, by wrapping the samples inside. While detailed mechanisms are still under investigation, the speculation is that the ability of graphene to rapidly conduct heat and charges can play a role.

The model system we chose to image here is 3D shaped Au–DNA artificial molecules, to study and quantify the effect of electron beam on the DNA molecules during the imaging process. Such artificial molecules can demonstrate: (1) the effect of the electron beam on DNA molecules, detected from the easily visible motions of Au nanoparticles (NPs); (2) determination of the 3D shape and dynamics of biomolecules that can be generalized to other small and low-contrast biomolecules. In addition, Au NPs inside the artificial molecules have plasmonic coupling that is sensitive to the construction of the artificial molecules. They have been extensively used as "plasmon rulers"[24–26] to detect the dynamics and activity of biomolecules, but their real 3D configuration in solution could not be easily probed. Imaging these artificial molecules in their working liquid environment is also crucial for optimizing the optical properties of their design for bio-sensing.

Experimental procedures

Gold NP preparation

Citrate-stabilized 5 nm gold NPs (83 nM) were purchased from Ted-Pella, Inc. (Redding, CA). We first stirred such NP solutions with an excess (1 mg BSPP per 1 mL deionized water) of bis(p-sulfanatophenyl)phenyl-phosphine (BSPP from Strem Chemicals, Inc., Newburyport, MA) overnight. Later, we collected the NPs, now coated with BSPP, by centrifuging the solution at 3000 rpm for 15 min. We then removed the supernatant solution and resuspended the NPs in BSPP solution (1 mg BSPP per 1 mL deionized water). Our stock solution was concentrated to 2 μM, and was kept at ambient temperature when not in use.

Preparation of single-stranded (ss) DNA

We obtained our ssDNA of desired lengths from Integrated DNA Technologies Inc. (Coralville, IA). The 5′ ends were modified with hexylthiol disulfide linkers, and then ssDNA were resuspended in 10 mM Tris buffer containing 0.5 mM EDTA in a ~100 μM concentration.

Preparation of Au–ssDNA conjugates

In one reaction, we mixed 70 μL stock solution of Au NPs, 1.5 μL ssDNA stock solution, 10 μL BSPP (5 mg mL^{-1} in deionized water), with 10 μL 500 mM NaCl solution, and had them react overnight without stirring at room temperature. The reaction mixture was then mixed with 10 μL of 20 mM poly(ethylene glycol) methyl ether thiol (MPEG) and reacted for 2 hours to replace the BSPP ligands on the Au NPs. The solution then went through high performance liquid chromatography (HPLC) to collect Au NPs with one and two ssDNA on the surface separately, depending on the desired nanoconjugate structure.

Preparation of trimers and pyramids

For trimers, Au NPs conjugated with two ssDNA were mixed and hybridized with Au–ssDNA monoconjugates twice in amount at room temperature overnight. Then reacted solution went through an Agarose gel (3 wt% in deionized water) in electrophoresis to obtain Au–ds DNA conjugates, trimers, from unreacted Au–ssDNA monoconjugate. The electrophoresis was done in 0.5× tris-borate-EDTA (TBE) buffer. The gels were run for 1 hour at 125 V, after which several distinct bands were visible. We extracted dimers, or trimers, by cutting the gel at the end of the proper band and immersing the gel piece in 0.5× TBE buffer and 200 mM NaCl solution. The obtained Au–double-stranded (ds) DNA nanoconjugate solution was stocked in the fridge when not in use. For pyramids, we followed the procedure in ref. 25, but used a DNA strand design such that one edge of the pyramids was shorter than the others.

Preparation of graphene covered TEM grids

The base TEM grids are Quantifoil R1.2/1.3300 Mesh Au holey carbon TEM grids purchased from SPI supplies. These TEM grids were pressed against graphene grown on Cu foil *via* chemical vapor deposition. A drop of isopropanol was cast on the Cu foil to immerse the pressed TEM grids to bind them with graphene as isopropanol evaporates. The Cu foil, with attached TEM grids facing up towards the air, was then placed on the surface of a sodium persulfate (Sigma Aldrich) solution (10 mg mL^{-1}), which etched away the Cu foil, leaving TEM grids coated with graphene. These TEM grids were subsequently rinsed with deionized water three times to wash off the etching solution, and were left to dry for further use.

Loading liquid sample into graphene liquid cell

We laid one graphene coated TEM grid onto a hard substrate such as a glass slide with the graphene side facing upwards. One tiny droplet (diameter ¼–$^1/_3$ of the TEM grid diameter) of the aqueous solution was deposited onto the center of the TEM grid. The other graphene coated TEM grid was then positioned on top to cover the bottom TEM grid and the droplet. During the slight evaporation of water after 10 min in the air, the top and bottom TEM grids were brought into close contact and kept the rest of the solution intact and sealed.

Microscopy

The TEM imaging was performed on LaB6 Tecnai G2 S-TWIN TEM at 200 kV. An accelerating voltage of 200 kV was used to obtain enough contrast and also to balance between avoiding damaging the graphene layer and lowering radiation damage. We set 0.1 seconds of exposure time and 0.9 seconds of read out time, therefore giving 1 second for the entire frame time, to acquire time-serial images.

Results

Graphene liquid cell imaging of 3D pyramidal artificial molecules

EM imaging of 3D structure and dynamics of biomolecules has two prerequisites: first, to be able to visualize low contrast, or sometimes invisible, biomolecules in morphological detail under EM, and second, to be able to obtain the 3D structure

of biomolecules from their 2D projections. Cryo EM developed staining methods using heavy metal ions to enhance the contrast, and thus the visibility, of biomolecules under EM. In addition, cryo EM relies on the homogeneity of biomolecules at a particular functional state to reconstruct the 3D structure of biomolecules from snapshots of millions of randomly oriented biomolecules. Using 3D shaped artificial molecules, we demonstrated our proposed strategies towards solving these two issues. The biomolecules, dsDNA, in the artificial molecules are too thin to be seen directly under TEM, and we show how the decoration of a specific staining agent, tiny Au NPs, can help capture the status of dsDNA and enable us to detect its conformational change. As to the 3D structure, instead of generating one structure from millions of molecules, we are able to obtain a series of 2D projections of one particular artificial molecule and to construct the 3D model accordingly.

Our 3D model artificial molecule is a pyramidal shape, with four Au NPs positioned at the vertices and dsDNA as the bridges. These pyramids are of the simplest geometric shape that extends into 3 dimensions, enabling multiplexed probing of distance or reaction dynamics along different directions. Moreover, the pyramidal arrangement mimics the atomic backbone of glyceraldehyde, the smallest commonly used chiral molecule. Theoretical calculations have predicted that such pyramidal artificial molecules, once their symmetry is broken, can generate circular dichroism signals in addition to the geometry-dependent back scatterings from coupled plasmons. Many experimental strategies were suggested to introduce such chirality in pyramids,[25] including using Au NPs of different sizes, or different dsDNA determined edge lengths. To allow the practical use of these artificial molecules beyond their use as model systems, we designed their DNA linker sequence such that the tetrahedral DNA constructs, if assembled and base-paired successfully, have one bond shorter than the others (see the red line in Fig. 1). This strategy, if successful, can serve as the first step towards more variations in DNA linker lengths that eventually generate chirality in the structure.

Conventional dry TEM imaging of the final assembled artificial molecules can show whether the Au NPs are in proximity, but cannot resolve their 3D arrangement in their native liquid environment, which is crucial to their optical properties and applications as biosensors. The backbone structure of the artificial molecules can be distorted during dry TEM sample preparation, due to the strong capillary force from the meniscus of the evaporating solvent. As shown in Fig. 2,
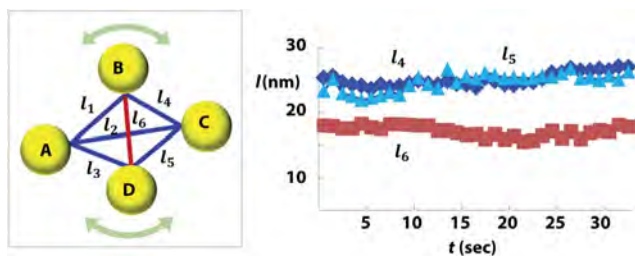

Fig. 1 3D remodeling of artificial pyramidal molecules. Left: the designed pyramidal molecule, with the red bond shorter than the other five blue bonds. Right: the calculated bond lengths for all the different frames (x axis).
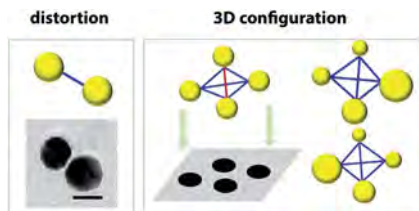
Fig. 2 Limitations of dry TEM imaging for artificial molecules. Left: the collapse of a dimeric artificial molecule. Right: the flattening of a pyramidal artificial molecule. Scale bar: 20 nm.

the component Au nanocrystals of a dimeric molecule were dragged closer together to a spacing of ~5 nm, despite the expected 15 nm dsDNA linker in between. Note that previous studies using small angle X-ray scattering[26] clearly demonstrated that, in the solution phase, the bond length of the same model dimeric molecules closely follows their linker length. It is therefore speculated that the capillary force can overwhelm the rigid linker and collapse their otherwise well-defined geometric configuration. Likewise, 3D artificial molecules get flattened onto the TEM grid, leaving hardly any information of their 3D configuration (see Fig. 2). This loss of 3D information poses a great challenge, since small angle X-ray, the alternative technique to probe the bond length between component artificial atoms, has difficulty interpreting 3D conformation data, not to mention that small angle X-ray can probe only the ensemble interparticle distances.

Using graphene liquid cell EM, we reconstructed the 3D configuration of pyramidal shaped artificial molecules in their native liquid environment. We sandwiched the solution of pyramids between two graphene layers and captured their dynamics under TEM. The Au NPs we used are small, around 5 nm in diameter, in order to minimize their effect on biomolecules as the "staining" agent. These small Au NPs can easily be seen under TEM, in comparison with the lower spatial resolution obtained from a thick-walled Si_3N_4 liquid chamber. We see this advantage of graphene liquid cell EM as crucial for the imaging of low-contrast biomolecules, as well as biomolecules stained with small high contrast agents. Here we watched one pyramid tumbling, due to the surrounding liquid environment, and recorded its continuous rotations as a TEM movie. Every snapshot in the movie has one 2D projection of the pyramid, and one set of six measurable projected distances between the four component Au NPs. This is our raw data, which can be obtained independently for every snapshot. We then employ the iterative optimization method described in detail in an earlier report from this laboratory.[13] In short, we assume three bond lengths as the inputs (see l_1, l_2, l_3 in Fig. 1), and calculate the 3D coordinates of particles B, C, D relative to particle A based upon the inputs and measured projected distances. Now that we have the 3D configuration of the pyramids, we further calculated the other unknown bond lengths (see l_4, l_5, l_6 in Fig. 1). We did the same calculation for each frame in a continuous movie, and optimized the three inputs until the variances of the three calculated bond lengths reach their minimums, which means the 3D configurations obtained from all the snapshots can converge into one structure.

Several observations can be concluded from this remodeling. The calculated bond lengths are consistent with our DNA design. As shown in the graph in Fig. 1 and representative TEM and 3D configurations shown in Fig. 3, one bond is indeed distinctly shorter than the other two bonds. The two longer bonds are also not only comparable with each other in length, but also comparable with the three input lengths. This consistency demonstrates that our solution phase-based DNA directed assembly into artificial molecules was able to introduce a bond length difference in the pyramidal shapes. More work is currently in progress to design a DNA sequence that can base pair into chiral pyramids for their unique optical properties. More importantly, this convergence into one 3D configuration of the pyramid indicates the geometric configuration of the pyramid stays intact during this time window of imaging. Otherwise, the pyramids will be distorted to different extents and to different shapes during the imaging process. This unique feature indicates the compatibility of graphene liquid cell TEM with imaging of other samples involving biomolecules and, eventually, even biomolecules themselves. The principle of imaging 3D shapes of biomolecules, although demonstrated here in the manner of "coarse-grained" staining, is shown in this example, and can be generalized to other biomolecules.

Electron beam effect

Interaction with the artificial molecules. Now that we have shown how a projected image relates to the 3D configuration of the pyramids, we can visualize the structural damage to the pyramids induced by electron beam in real time. During TEM imaging of biomolecules, the electron beam has been found to induce dramatic structure changes through ionization and consequently bond
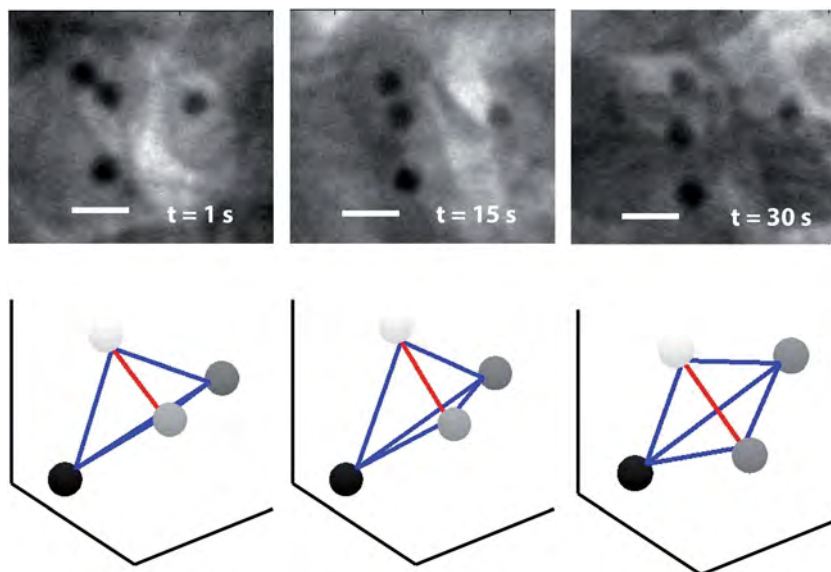

Fig. 3 Snapshots of a continuous TEM movie (top) and the corresponding 3D models (bottom). Scale bars are 10 nm. The spheres in the 3D models are color coded according to their z height.

breakage and bond rearrangements. Extensive studies have been done for biomolecules at cryogenic temperatures, showing that radiation damage is reduced significantly when biomolecules are embedded in a layer of vitrified ice, with the limitation that the samples are also locked in place and become stationary.

Recent EM imaging of a liquid phase sample has started to suggest new mechanisms for lowering such radiation damage and allowing imaging of biomolecules at higher spatial resolution and for longer observation time. Reports using Si_3N_4 liquid cell EM techniques[6,8,10,12] argued that the native liquid environment significantly attenuates the structural distortion of bio-samples, including both proteins and living cells, under continuous exposure to the electron beam. The use of graphene in this context for static yet hydrated ferritin[9] and bacteria[7,11] has also shown lowering of radiation damage, possibly by rapid conductance of heat and charges. Due to the complicated origins of electron beam damage, the mechanisms for such a reduction of the electron beam effect have not been thoroughly investigated. In some cases, seemingly controversial observations were reported about the nature of radiation damage, dose dependent or dose rate dependent, and about the state of the liquid environment under electron beam, dried out or truly hydrated. Our observation of a dynamic pyramid in the graphene liquid cell can serve as a good control system for further investigation into the electron beam effect.

We followed the pyramidal artificial molecule used in our 3D remodeling for a prolonged time and found it suffered dramatic structural deformation after 40 seconds of exposure to the electron beam. As highlighted in Fig. 4, the distance between particles A and B became abruptly large; particle B later diffuses away from the other three component Au NPs. This observation has several indications. The connection between particles A and B was broken once the accumulated electron dose reached a threshold value. Such dose dependent radiation damage is consistent with the previous studies. This dose threshold is larger than that determined from cryogenic TEM imaging of biomolecules,[1] but comparable with
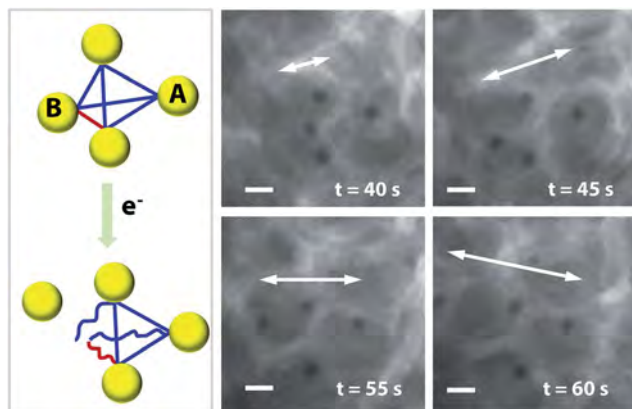

Fig. 4 The breakage of DNA linkage after imaging the pyramid shown in Fig. 2 and 3 for a longer time. Left: schematics. Right: TEM series, where the arrows highlighted the distance between particles A and B. Scale bar is 10 nm.

the reported increased thresholds in both Si_3N_4 and graphene liquid cell experiments.[6–8,10–12] Meanwhile, this transition from a converged 3D pyramidal shape to a dissembled structure proves in return that the pyramidal structure was indeed in liquid and that the positions of the Au NPs fully described the 3D conformation of the pyramids.

It is still an open question if the deformed pyramids truly indicate in real time the structural damage to dsDNA in the graphene liquid cell. It is very probable that the breakage of individual bonds in DNA molecules occurs prior to the loss of the connecting capability of the DNA chains, therefore prior to the observed phenomenon of Au nanocrystals. Several reasons can lead to this possible gap between the apparent critical dose and the real critical dose for biomolecules. Nanoscale objects have been repeatedly found to have slowed motions[18,21] within the liquid cell configuration. This sluggish motion may effectively act like a "cage" that keeps the structure from diffusing apart altogether, even after the linkage is broken. For the imaging of artificial molecules, this mechanism is efficient enough, as we shown earlier in the text, for us to remodel their 3D conformation.

Of course our use of visual markers, the Au NPs, makes our probing of the DNA molecules indirect. A more vigorous and quantitative experiment will be the direct visualization of high-contrast biomolecules, to quantify and capture the critical dose at which the structural details of biomolecules start to blur or to degrade. Both high-contrast biomolecules, ribosomes for example, and heavy metal ion-stained biomolecules can be good candidate systems to show if there is a quantitative improvement in the dosage tolerance of biomolecules when using graphene liquid cells.
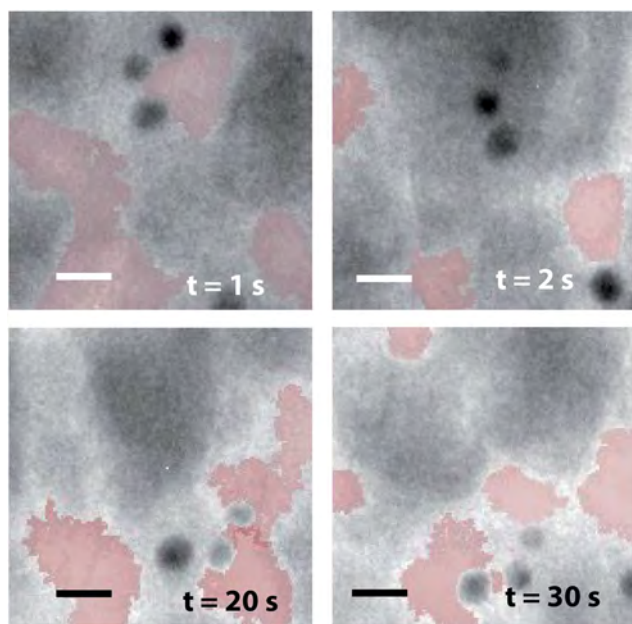

Fig. 5 Snapshots of a continuous TEM movie of a trimeric artificial molecule. Red shadows highlight areas of high intensity. Scale bar: 6 nm.

Interaction with the liquid medium. One unique aspect inherent to all liquid cell EM experiments is that the electron beam can also interact with the liquid medium in addition to the sample of interest.[19] Previous studies have been focused on possible radiation chemistries, where electron beam can produce reactive species to initiate chemical reactions *in situ*.

We have looked into another frequently observed phenomenon: the intensity fluctuation of the liquid environment during the liquid cell imaging. As shown in Fig. 5, artificial trimeric molecules rotate in the series of TEM images, together with a visible background fluctuation. One can clearly see the distinct lighter and darker islands in the surrounding liquid environment, with the lighter domains highlighted by red shadows in the TEM images. The positions of the red domains relative to those of the trimers randomize from frame to frame, exhibiting little correlation with the motion of the trimers. In other words, the motions of the trimers are independent of the dynamic fluctuation of the liquid environment, which indicates a lower possibility of the background fluctuation being of a convection nature. This lack of correlation, although the origin of the fluctuation is still not resolved, is important since the motions, and consequently the imaged configurations, of the nanocrystals are not then disturbed by the instantaneous flow pattern of the solution.

Conclusions and outlook

The development of bio-imaging techniques has been associated with important scientific understandings of structures and functions of living systems, and practical applications such as diagnosis and drug engineering. We discussed and demonstrated the unprecedented advantages brought by the recently developed graphene liquid cell EM as a new method of bio-imaging. Graphene liquid cells have a unique combination of properties: they provide both the native liquid environment enabled by optical microscopy and the nanometer resolution enabled by electron microscopy. This combination can potentially answer questions that were previously simply not approachable by other experimental techniques, such as the structures of membrane proteins in action in their working environment, the conformational docking of drugs at target proteins, and eventually the real nanoscale imaging of biomolecules functioning and in motion. In the paper, we used Au NP–DNA artificial molecules, which are frequently employed for the detection of a biomolecular environment, as model systems to illustrate how we can work with the challenges of bio-imaging using graphene liquid cells. We were able to generate 3D shapes of a certain artificial molecule by following its series of 2D projections through continuous rotations. Note that, previously, people have had to either rely on the monodispersity of millions of biomolecules (cryo EM) or on the bulk crystalline form of biomolecule crystals (X-ray crystallography) to do 3D reconstruction. In addition, we show how the small "staining" agents we used to make the invisible biomolecules visible are clearly imaged under graphene liquid cell EM, a unique capability of holding liquid samples in between two ultrathin graphene layers, rather than other thicker microfabricated chips. Furthermore, based upon these two capabilities, we followed the structural damage of artificial molecules under the imaging electron beam and found that the structural backbone of artificial molecules was kept stable under a higher electron dose than the previously determined threshold.

Although the stability of the artificial molecules may be different from the stability of their biomolecular linkers, more studies from other groups have also shown that graphene wraps can protect both dry and aqueous samples under an electron beam. This protection mechanism, if fully quantified and understood, can have a huge impact beyond the graphene liquid cell EM technique itself. For example, conventional cryo EM could potentially use graphene wraps to make samples more stable and allow better contrast under the imaging beam.

Acknowledgements

References

1 L. F. Kourkoutis, J. M. Plitzko and W. Baumeister, *Annu. Rev. Mater. Res.*, 2012, **42**, 33.

2 J. N. Onuchic and P. G. Wolynes, *Curr. Opin. Struct. Biol.*, 2004, **14**, 70.

3 A. Pulk and J. H. D. Cate, *Science*, 2013, **340**, 1235970.

4 J. W. Miao, H. N. Chapman, J. Kirz, D. Sayre and K. O. Hodgson, *Annu. Rev. Biophys. Biomol. Struct.*, 2004, **33**, 157.

5 K. Xu, G. Zhong and X. Zhuang, *Science*, 2013, **339**, 452.

6 U. M. Mirsaidov, H. Zheng, C. Yosune and P. Matsudaira, *Biophys. J.*, 2012, **102**, L15.

7 F. Banhart, *ChemPhysChem*, 2011, **12**, 1637.

8 M. T. Proetto, *et al.*, *J. Am. Chem. Soc.*, 2014, **136**, 1162.

9 C. Wang, Q. Qiao, T. Shokuhfar and R. F. Klie, *Adv. Mater.*, 2014, **26**, 3410.

10 D. B. Peckys and N. de Jonge, *Nano Lett.*, 2011, **11**, 1733.

11 N. Mohanty, M. Fahrenholtz, A. Nagaraja, D. Boyle and V. Berry, *Nano Lett.*, 2011, **11**, 1270.

12 S. M. Hoppe, D. Y. Sasaki, A. N. Kinghorn and K. Hattar, *Langmuir*, 2013, **29**, 9958.

13 Q. Chen, J. M. Smith, J. Park, K. Kim, D. Ho, H. I. Rasool, A. Zettl and A. P. Alivisatos, *Nano Lett.*, 2013, **13**, 4556.

14 S. van de Linde, M. Heilemann and M. Sauer, *Annu. Rev. Phys. Chem.*, 2012, **63**, 519.

15 T. J. Gould, S. T. Hess and J. Bewersdorf, *Annu. Rev. Biomed. Eng.*, 2012, **14**, 231.

16 J. M. Yuk, *et al.*, *Science*, 2012, **336**, 61.

17 N. de Jonge and F. M. Ross, *Nat. Nanotechnol.*, 2011, **6**, 695.

18 J. Lu, Z. Aabdin, N. D. Loh, D. Bhattacharya and M. Utkur, *Nano Lett.*, 2014, **14**, 2111.

19 J. M. Grogan, N. M. Schneider, F. M. Ross and H. H. Bau, *Nano Lett.*, 2014, **14**, 359.

20 H.-G. Liao, L. Cui, S. Whitelam and H. Zheng, *Science*, 2012, **336**, 1011.

21 H. Zheng, S. A. Claridge, A. M. Minor, A. P. Alivisatos and U. Dahmen, *Nano Lett.*, 2009, **9**, 2460.

22 R. Zan, Q. M. Ramasse, R. Jalil, T. Georgiou, U. Bangert and K. S. Novoselov, *ACS Nano*, 2013, **7**, 10167.

23 G. Algara-Siller, S. Kurasch, M. Sedighi, O. Lehtinen and U. Kaiser, *Appl. Phys. Lett.*, 2013, **103**, 203107.

24 S. E. Lee, A. P. Alivisatos and M. J. Bissell, *Systems Biomedicine*, 2013, **1**, 12.

25 A. J. Mastroianni, S. A. Claridge and A. P. Alivisatos, *J. Am. Chem. Soc.*, 2009, **131**, 8455.

26 A. J. Mastroianni, D. A. Sivak, P. L. Geissler and A. P. Alivisatos, *Biophys. J.*, 2009, **97**, 1408.